Experimental and numerical studies of concrete-filled high-chromium stainless steel tube (CFHSST) stub columns

An He [a], Fangying Wang [b], Ou Zhao [*c]

[a, b, c] School of Civil and Environmental Engineering, Nanyang Technological University, Singapore

[*] Corresponding author, Phone: +65 6790 6934

Email: ou.zhao@ntu.edu.sg

Abstract: The present paper reports a thorough experimental and numerical investigation into the compressive behaviour and load-carrying capacities of concrete-filled steel tube (CFST) stub columns with the outer tubes made of a newly developed high-chromium grade EN 1.4420 stainless steel. In comparison with the most commonly used stainless steel grades EN 1.4301 and EN 1.4404, the new grade EN 1.4420 possesses lower material price, but better corrosion resistance and higher strength, and thus has a greater potential for widespread use in composite construction. In this study, an experimental programme was firstly carried out on 15 CFST stub columns with high-chromium stainless steel tubes of five different cross-section sizes and concrete infill of three grades, as well as 5 (reference) bare high-chromium stainless steel tube stub columns. The test setup, procedure and results, including the ultimate loads, load–deformation histories and failure modes, were fully reported. The experimental investigation was supplemented by a numerical modelling study, where the developed finite element models were firstly validated against the experimentally obtained results and then utilised to perform parametric studies for the purpose of expanding the limited test data pool over a wider range of cross-section sizes. The test and numerical results were utilised to evaluate the applicability of the codified provisions, established in North America, Europe and Australia, to the design of the new concrete-filled high-chromium stainless steel tube stub columns. Overall, the examined design codes were generally found to yield safe-sided but slightly conservative resistance predictions for the new high-chromium stainless steel composite stub columns. Modifications to the codified design provisions were then made, and shown to result in an improved level of design accuracy.

1. Introduction

The past decades have been witnessing an extensive application of concrete-filled steel tube (CFST) composite columns over the conventional reinforced concrete and bare steel columns in civil and offshore engineering practices, owing to their more favourable structural performance, including higher load-carrying capacity, larger stiffness, and better seismic and cyclic behaviour. For example, CFST columns are widely employed as vertical load-bearing components to hold up the whole structure systems in high-rise buildings and as piers to support beam girders in long-span bridges. However, despite CFST members possessing high load-

carrying capacities, their resistances against corrosion are almost negligible, due to the fact that the outer carbon steel tubes, directly exposed to air and water, are rather vulnerable to corrosion. Therefore, regular maintenance such as the spray of anti-corrosive coatings on the outer carbon steel tubes is generally required over the whole service life of CFST structures, resulting in significant additional costs and inspection work. There is thus an increasing trend of utilising corrosion-resistant stainless steel tubes to replace the conventional carbon steel tubes in the fabrication of CFST composite columns. In comparison with carbon steel, which exhibits a linear elastic region and a clear yield point, followed by a yield plateau and then some strain hardening, stainless steel displays a distinctive nonlinear and ductile material response with a high level of strain hardening, thus leading to stainless steel–concrete composite columns with different structural behaviour from their carbon steel–concrete composite counterparts. This has prompted a series of experimental studies on concrete-filled stainless steel tube (CFSST) column members, aimed at verifying their unique structural behaviour and quantifying the corresponding load-carrying capacities in compression. Specifically, stub column tests were carried out on square [1-4], rectangular [2-4] and circular [1, 3] normal strength concrete-filled stainless steel tubes, to investigate their cross-section compression resistances and the effect of cross-section shape on the development of confining stress during the loading process, while the structural performance of CFSST stub columns with novel types of concrete infill, such as recycled aggregate concrete and seawater and sea sand concrete, were respectively studied by Yang and Ma [5] and Li et al. [6, 7], based on a thorough testing programme. Uy et al. [1], Ellobody and Ghazy [8] and Tokgoz [9] performed experimental studies on both normal strength and fibre reinforced concrete-filled stainless steel tube long columns, and examined their flexural buckling behaviour and resistances. Fire tests on normal strength concrete-filled stainless steel tube long columns were reported in Han et al. [10] and Tao et al. [11], where the reduced strengths of CFSST long columns at elevated temperatures were investigated and quantified, while the post-fire residual strengths of normal strength concrete-filled stainless steel tube stub columns were experimentally studied by Chen et al. [12]. It has been verified from previous experimental studies [1-12] that stainless steel composite columns have generally more ductile structural responses and higher load-carrying capacities at both room and elevated temperatures and after exposure to fire than their carbon steel counterparts, owing principally to the more favourable material characteristics of stainless steel.

The excellent mechanical properties, coupled with the corrosion-resistant nature, make stainless steel a potentially attractive and promising construction material in composite structures; however, its actual application is generally hindered by the high material price, which is around four times that of carbon steel. Therefore, new stainless steel grades with lower material price but even more favourable mechanical properties and higher corrosion resistances continue to be developed, with a recent example being a novel high-chromium austenitic stainless steel - grade EN 1.4420 [13-15]. Table 1 reports the chemical compositions of the two most commonly used stainless steel grades EN 1.4301 and EN 1.4404 as well as the new grade EN 1.4420 [13,16]. It is worth noting that the material price of stainless steel is mainly dependent on the nickel content, while the material strength and corrosion resistance are associated with the contents of chromium and nitrogen. Therefore, in comparison with the two most commonly used stainless steel grades EN 1.4301 and EN 1.4404, the new grade EN

1.4420 has lower material price, owing to the lower nickel content, but better corrosion resistance and higher strength, due to the higher contents of chromium and nitrogen, indicating a greater potential for widespread use in composite construction.

A research project is currently being carried out at Nanyang Technological University to systematically investigate the structural behaviour of the novel concrete-filled high-chromium stainless steel tube (CFHSST) composite members, with an experimental and numerical study on square and rectangular CFHSST stub columns reported in the present paper. An experimental programme, which comprises material testing, including high-chromium stainless steel tensile flat and corner coupon tests and concrete cylinder tests, and twenty concentrically loaded stub column tests, was firstly carried out and described. This was followed by a numerical modelling programme, where finite element models were firstly developed and validated against the CFHSST stub column test results, and then utilised to perform numerical parametric studies to expand the experimental data pool on CFHSST stub columns over a wider range of cross-section sizes. The applicability of the codified provisions for concrete-filled carbon steel tube stub columns, as given in the American Specification AISC 360-16 [17], European code EN 1994-1-1 [18] and Australian standard AS 5100 [19], to the design of the new high-chromium stainless steel composite stub columns was evaluated, based on the experimentally and numerically derived data. Modifications to the codified design provisions were also made.

2. Experimental investigation

2.1 General

A testing programme was firstly performed, to derive an experimental data pool on concrete-filled high-chromium stainless steel tube (CFHSST) stub columns. In the present experimental study, three square hollow sections (SHSs) and two rectangular hollow sections (RHSs) made of the new high-chromium grade EN 1.4420 stainless steel were adopted for fabricating the composite stub column specimens: SHS 100×100×3, SHS 120×120×5, SHS 150×150×5, RHS 100×50×5 and RHS 150×100×5, which were manufactured by gas-shielded metal arc welding of two press-braked channel sections at the flange tips (see Fig. 1). For each of the five adopted cross-sections (corresponding to five specimen series), concrete infill of three grades, namely C40, C60 and C80 was used, leading to a total of 15 CFHSST stub columns. In addition, five unfilled (bare) stainless steel tube stub column reference specimens were also prepared. The nominal length of each of the composite and bare stainless steel stub column specimens was selected to be three times the larger dimension of the cross-section, in order to prevent the occurrence of member global instability [2, 20]. The labelling system of the CFHSST stub column specimens consists of the nominal cross-section dimensions of the outer high-chromium stainless steel tube and the material grade of the inner concrete, e.g., SHS 120×120×5-C40 and SHS 120×120×5-C0; note that 'C0' denotes bare high-chromium stainless steel tube stub column specimen without concrete infill. Table 2 lists the measured dimensions of the concrete-filled and bare high-chromium stainless steel tube stub column specimens, where h, b, t and r_i are the overall depth and width, thickness and inner corner radius

of the outer stainless steel tube, respectively, and L is the member length. The cross-section areas of the outer high-chromium stainless steel tube and inner concrete core (denoted as A_s and A_c, respectively) for each specimen were also calculated and reported in Table 2.

2.2 Material testing

Prior to stub column tests, tensile coupon tests and standard cylinder tests were respectively performed to derive the material properties of both the outer high-chromium stainless steel tubes and the inner concrete cores of the CFHSST specimens. For each high-chromium stainless steel tube section size, one flat coupon was cut along the centreline of the face containing no welds (see Fig. 1), and one additional corner coupon was extracted from the curved corner portion; the dimensions of both the flat and corner coupons are in compliance with the geometric requirements specified in EN ISO 6892-1 [21]. Tensile coupon tests were carried out using a 250 kN hydraulic testing machine under displacement-control. Specifically, the initial loading rate was set to be equal to 0.05 mm/min prior to the material nominal 0.2% proof stress of 320 MPa, and followed by an increased loading rate of 0.8 mm/mm until the fracture of the tensile coupons; the resulting strain rates satisfied the relevant requirements given in EN ISO 6892-1 [21]. Fig. 2 displays the tensile coupon test rig, including an extensometer with the gauge length of 50 mm mounted onto the middle portion of the necked part of the coupon and a pair of strain gauges affixed to the mid-height of the coupon. The measured material stress−strain curves for the flat and corner coupons extracted from the five studied high-chromium stainless steel tube sections are shown in Fig 3, while the key measured material properties, including the Young's modulus E, the 0.2% proof stress $\sigma_{0.2}$, the ultimate stress σ_u, the strain at the ultimate stress ε_u, and the strain hardening exponents (n and m) adopted in the Ramberg−Osgood material model [22-26] for representing the nonlinear material stress−strain response of stainless steel, are reported in Table 3.

Concrete infill of three grades (C40, C60 and C80) was employed to fabricate the CFHSST stub column specimens. The concretes were produced using the CEM I 52.5N Portland cement, river sand, gravel with the maximum aggregate size of 10 mm, silica fume, superplasticizer, and fresh water, with the detailed mix designs given in Table 4. For each of the three concrete grades, four concrete cylinders were casted, with the dimensions following the recommendations in BS EN 12390-3:2009 [27], and then cured along with the CFHSST stub columns under the same condition. Standard cylinder tests were carried out at the time of the CFHSST stub column tests. The average measured compressive cylinder strengths f_c for the C40, C60 and C80 concretes were equal to 49.1 MPa, 68.1 MPa and 86.4 MPa, respectively, with the corresponding coefficients of variation (COVs) of 0.01, 0.05 and 0.02. Upon derivation of the material properties of high-chromium stainless steel and concrete, the confinement factor ξ [1, 28], which is an index reflecting the potential level of lateral confinement provided by the outer tube to the inner concrete, can be determined from Eq. (1) for each of the CFHSST stub column specimens, as reported in Table 2.

$$\xi = \frac{\sigma_{0.2} A_s}{f_c A_c} \tag{1}$$

2.3 Stub column tests

In total, 20 concentric compression tests were carried out on concrete-filled and bare high-chromium stainless steel tube stub columns to investigate their structural behaviour and load-carrying capacities subjected to axial compressive force. A 5000 kN hydraulic testing machine with fixed platens at both ends, driven by displacement-control at a constant speed of 0.3 mm/min, was adopted for the stub column tests. Prior to the testing, a thin layer of gypsum was applied to both ends of the CFHSST stub column specimens and then hardened between two flat rigid platens under a small load of 5 kN; this ensured the achievement of flat end surfaces of the specimens, and thus a uniform compressive stress distribution on both the outer high-chromium stainless steel tube and inner concrete core during the tests. Fig. 4 depicts the stub column test setup, where a series of G-clamps are utilised at both ends of the specimen, to prevent any occurrence of local failure at the specimen ends, four linear variable differential transducers (LVDTs) are employed for measuring the axial shortening of the specimen, and a pair of strain gauges are affixed to the mid-height of the outer high-chromium stainless steel tube of the specimen to record the longitudinal strains during the loading process.

The experimental load–end shortening curves for each specimen series (i.e. CFHSST stub columns with the same outer high-chromium stainless steel tube size) are shown in Figs 5(a)–5(e), respectively, while the key obtained experimental results, including the ultimate load $N_{u,test}$ and the corresponding end shortening at the ultimate load δ_u, are summarised in Table 5. Note that for CFHSST stub column specimens with relatively stocky outer tube sections and low concrete grades (for example, specimen RHS 100×50×5-C40), the load–deformation responses were flat even at unrealistically large plastic deformations, and the corresponding experimental ultimate loads were taken as the loads where the tangent stiffnesses of the load–end shortening curves were equal to 1% of the initial stiffnesses [29]. Figs 6 and 7 depict the failure modes of typical CFHSST stub column specimens SHS 100×100×3-C40 and RHS 150×100×5-C40, featuring outward local buckling of the outer stainless steel tubes, accompanied by crushing of the inner concrete.

The ductility of the steel and composite stub columns was evaluated by the ductility index (*DI*) [28, 30, 31], which is defined as the ratio of the end shortening at which the post-ultimate path of the load–end shortening curve drops to 85% of the ultimate load ($\delta_{85\%}$) to the end shortening corresponding to the ultimate load (δ_u), as given by Eq. (2). The ductility indices of the concrete-filled high-chromium stainless steel tube stub column specimens are reported in Table 5, and also found to be generally higher than those of the carbon steel composite stub columns, owing principally to the favourable material characteristics of the high-chromium grade EN 1.4420 stainless steel tubes (including high strain hardening and large ductility). The ductility indices of two typical specimen series - CFHSST stub columns with the outer tubes of SHS 100×100×3 and RHS 150×100×5 - are plotted against the measured concrete cylinder strengths in Fig. 8. The results of the comparisons clearly show that (i) the use of high strength concrete is associated with a reduction in member ductility, and (ii) composite specimens with more

stocky outer tubes (e.g., specimen series with the outer tube of RHS 150×100×5) display higher ductility than those with less stocky outer tubes (e.g., specimen series with the outer tube of SHS 100×100×3).

$$DI = \frac{\delta_{85\%}}{\delta_u} \tag{2}$$

3. Numerical simulation

3.1 General

The experimental study, presented in Section 2, was supplemented by a numerical simulation investigation, carried out using the finite element (FE) analysis software ABAQUS [32] and reported in this section. The techniques and assumptions relevant to the development of CFHSST stub column FE models were fully described. Validation of the developed FE models was conducted by comparing the numerically obtained results against the corresponding experimental observations. This was then followed by a series of parametric studies, performed based on the validated FE models, to expand the derived experimental data pool on CFHSST stub columns over a wider range of cross-section dimensions.

3.2 Development of FE models

Finite element models were developed using the measured cross-section dimensions and lengths of the CFHSST stub column specimens reported in Table 2. The four-node shell element S4R and eight-node brick element C3D8R [32] have been extensively utilised in previous numerical modelling [1, 11, 30, 33-35] of the outer thin-walled stainless steel tubes and inner solid concrete cores of concrete-filled stainless steel tube composite columns, respectively, and were thus also employed in the present numerical simulations of CFHSST stub columns. The sizes of both the shell element S4R and brick element C3D8R were taken as 1/20 of the mean cross-section dimension of the specimen, i.e. 0.5(h+b)/20, following a mesh convergence study with the examined element sizes ranging from 0.5(h+b)/50 to 0.5(h+b)/5.

The plastic material model with isotropic hardening, as provided in ABAQUS [32] for metallic material, was employed for the material modelling of high-chromium stainless steel tubes, while the material stress–strain response of concrete was represented by the concrete damage plasticity (CDP) model in ABAQUS [32]. The elastic modulus and Poisson's ratio of concrete were respectively taken as $4700\sqrt{f_c}$ and 0.2 [36], while the parameters related to the plasticity of concrete, including the dilation angle ψ, flow potential eccentricity e, the ratio of the second stress invariant on the tensile meridian to that on the compressive meridian K_c, the ratio of the compressive strength under biaxial loading to the uniaxial compressive strength f_{b0}/f_c and the viscosity parameter μ, were calculated in accordance with the recommendations given in Tao et al. [37]. To consider the beneficial effect of confinement provided by the outer high-chromium stainless steel tube to the inner concrete core, an equivalent uniaxial

compressive stress–strain response, derived from the confined concrete model proposed by Tao et al. [37], was inputted into the CDP model. The tensile stress–strain relationship of concrete is assumed to be linear elastic up to the concrete tensile strength of $0.1f_c$, followed by an inelastic post-ultimate material response, characterised by means of fracture energy (G_F) [38].

The interaction between the outer high-chromium stainless steel tube and inner concrete core was simulated by means of the surface-to-surface contact [1, 11, 30, 33-35]. The outer surface of the solid concrete core and the inner surface of the thin-walled stainless steel tube were respectively selected as the 'master surface' and 'slave surface'. In the normal direction, a hard contact pressure–overclosure relationship was adopted, allowing for separation of the two interfaces in tension, but with no penetration in compression, while the tangential behaviour between the two interfaces was defined through a penalty method with the friction coefficient set to be equal 0.25 [33]. Moreover, the two end sections of each CFHSST stub column FE model were fully restrained except for the longitudinal translation at one end, in order to achieve the same fixed-ended boundary condition adopted in the stub column tests. For concrete-filled steel tube stub columns, the initial local geometric imperfections of the outer tubes have minimal effect on their local buckling behaviour and load-carrying capacities [33, 34], and thus incorporation of the initial local geometric imperfections of the outer high-chromium stainless steel tubes into the CFHSST stub column FE models was deemed unnecessary. For bare (unfilled) high-chromium stainless steel tube stub columns, the initial local geometric imperfections were explicitly included into the corresponding FE models in the form of the lowest elastic critical local buckling mode shapes under axial compression, with the maximum amplitudes predicted by the modified Dawson and Walker (D&W) model [38, 39].

3.3 Validation of FE models

Upon development of the CFHSST stub column FE models, nonlinear analysis was conducted to derive the numerical failure loads, load–end shortening curves and failure modes, which were then compared against the corresponding experimentally obtained results, allowing the accuracy of the developed numerical models to be evaluated. Table 5 presents the ratios of FE to experimental failure loads $N_{u,test}/N_{u,FE}$ for the CFHSST stub column specimens; the results of the comparisons indicate that the developed numerical models yield a high degree of accuracy and consistency in predicting the experimental ultimate loads. Comparisons between the test and FE load–end shortening curves for all the five specimen series are displayed in Figs 5(a)–5(e), where the initial stiffnesses, failure loads and general shapes of the experimental load–deformation responses are shown to be fully captured by numerical modelling. Excellent agreement is also obtained between the experimental and FE failure modes, as illustrated in Figs 6 and 7. To conclude, the finite element models developed in Section 3.2 are capable of precisely simulating the CFHSST stub column tests, and thus considered to be validated.

3.4 Numerical parametric studies

Upon validation of the finite element models in Section 3.3, numerical parametric studies were performed to generate further structural performance data on CFHSST stub columns over a broader range of cross-section dimensions. In the present parametric studies, the measured flat and corner material properties of the high-chromium stainless steel SHS 150×150×5 were adopted for the outer tubes of the modelled CFHSST stub columns, while three grades of concrete infill C40, C60 and C80 with the measured cylinder strengths respectively equal to 49.1 MPa, 68.1 MPa and 86.4 MPa were utilised for the inner concrete cores. In terms of the cross-section dimensions, the outer widths of the modelled high-chromium stainless steel tubes b were fixed at 100 mm, while five outer section depths h, respectively equal to 100 mm, 125 mm, 150 mm, 175 mm and 200 mm, were employed, leading to a range of cross-section aspect ratios from 1.0 mm to 2.0 being considered. The thickness and inner radius of each modelled high-chromium stainless steel tube section were set to be equal, and varied between 1.25 mm and 13.33 mm, with the resulting h/t ratios varying between 15 and 80. In sum, 210 numerical parametric study results on CFHSST stub columns were generated.

4. Assessment of existing design codes and modifications to the codified design provisions

4.1 General

Given that there have been no established design standards for stainless steel–concrete composite structures, the corresponding design provisions for concrete-filled carbon steel tube stub columns, as set out in the American Specification AISC 360-16 [17], European code EN 1994-1-1 [18] and Australian standard AS 5100 [19], were evaluated for the new concrete-filled high-chromium stainless steel tube stub columns. The shortcomings of the codified design approaches were highlighted, and revised design rules were then proposed, underpinned by and validated against the derived experimental and FE results. Table 6 presents the mean ratios of the test and numerical ultimate loads to the (unfactored) predicted ultimate loads $N_u/N_{u,pred}$ for all the examined design codes as well as the revised approaches.

4.2 AISC 360-16 [17]

The design cross-section compressive resistance of a square or rectangular concrete-filled carbon steel tube stub column, given in the American specification AISC 360-16 [17], is dependent on the class of the outer steel tube section. Three classes of square or rectangular hollow sections with concrete infill, namely compact section, non-compact section and slender section, are defined through comparing the flat width-to-thickness ratio $\lambda=c/t$ of the most slender constituent plate element of the section against the limiting slendernesses between compact and non-compact sections and between non-compact and slender sections (denoted as $\lambda_p = 2.26\sqrt{E/f_y}$ and $\lambda_r = 3.00\sqrt{E/f_y}$, respectively). For compact concrete-filled steel tube sections with $\lambda<\lambda_p$, the outer steel tube is capable of reaching the material yield stress f_y at

failure and also providing sufficient confinement to the inner concrete to achieve its effective compressive strength of $0.85f_c$, leading to the expression for the calculation of cross-section compression resistances given in Eq. (3). Non-compact steel tube sections with $\lambda_p \leq \lambda < \lambda_r$ are still assumed to attain the material yield stress at failure, but cannot offer sufficient confinement to enable the concrete infill to reach the effective compressive strength, with the design formulation for cross-section compression resistances of non-compact CFST stub columns given in Eq. (4). Slender tube sections with $\lambda \geq \lambda_r$ suffer from local buckling prior to the attainment of the material yield stress at failure, and are also unable to provide efficient confinement to the inner concrete core; this respectively limits the design stresses of the steel tube and concrete infill to the elastic critical buckling stress f_{cr} and $0.7f_c$, leading to Eq. (5) for cross-section resistances of CFST stub columns with slender tube sections.

$$N_{u,AISC} = f_y A_s + 0.85 f_c A_c \quad \text{for } \lambda < \lambda_p \tag{3}$$

$$N_{u,AISC} = f_y A_s + 0.85 f_c A_c - \frac{0.15 f_c A_c}{(\lambda_r - \lambda_p)^2}(\lambda - \lambda_p)^2 \quad \text{for } \lambda_p \leq \lambda < \lambda_r \tag{4}$$

$$N_{u,AISC} = f_{cr} A_s + 0.7 f_c A_c \quad \text{for } \lambda \geq \lambda_r \tag{5}$$

The applicability of the AISC 360-16 design rules to CFHSST stub columns was assessed through comparing the predicted compression resistances against the experimental and numerical results. The AISC compression resistances of CFHSST stub columns were determined herein using Eqs (3)–(5), but with the stainless steel material 0.2% proof stress $\sigma_{0.2}$ replacing the carbon steel yield stress f_y, i.e. $f_y=\sigma_{0.2}$. The mean test (or FE) to AISC predicted resistance ratio $N_u/N_{u,AISC}$, as reported in Table 6, is equal to 1.155, with the corresponding COV of 0.043, indicating that the AISC design rules for carbon steel composite stub columns can be safely applied to their high-chromium stainless steel counterparts, but with conservative resistance predictions.

4.3 EN 1994-1-1 (EC4) [18]

The EC4 cross-section compression resistance of a square or rectangular CFST stub column is given as the summation of the resistances of the outer steel tube and the concrete infill, as defined by Eq. (6), where A_d is the design cross-section area of the outer carbon steel tube, and taken as the gross area A_s for non-slender tube sections with the geometric dimensions of the constituent plate elements falling within the limit λ_{EC4} given by Eq. (7), but calculated as the effective area A_{eff} for slender tube sections susceptible to local buckling, based on the effective width method. It is worth noting that the Young's modulus of stainless steel ranges from 180000 MPa to 220000 MPa, and is thus different to the fixed value of 210000 MPa of carbon steel. Therefore, in the present study on CFHSST stub columns, Eq (7) was modified for stainless steel to reflect the difference in Young's modulus, as given by Eq (8). Moreover, the effective width formulation provided in EN 1993-1-4 [40] for slender stainless steel internal plate elements was adopted herein to calculate the reduction factor in plate element width due to local buckling ρ, as shown in Eq. (9), where $\bar{\lambda}_p$ is the plate element slenderness and can

be determined from Eq. (10), in which v=0.3 is the Poisson's ratio for stainless steel, and k is the buckling coefficient and equal to 4 for internal plate element in pure compression; note k=4 was originally derived for uniformly compressed simply-supported plates with a two-way elastic critical local buckling mode.

$$N_{u,EC4} = f_y A_d + f_c A_c \tag{6}$$

$$\frac{c}{t} \le \lambda_{EC4} = 52\left(\frac{235}{f_y}\right)^{0.5} \tag{7}$$

$$\frac{c}{t} \le \lambda_{EC4} = 52\left(\frac{235}{\sigma_{0.2}}\frac{E}{210000}\right)^{0.5} \tag{8}$$

$$\rho = \frac{0.772}{\bar{\lambda}_p} - \frac{0.079}{\bar{\lambda}_p^{\,2}} \quad \text{for } \bar{\lambda}_p > 0.65 \tag{9}$$

$$\bar{\lambda}_p = \sqrt{\frac{12(1-\upsilon^2)\sigma_{0.2}}{k\pi^2 E}}\,(c/t) \tag{10}$$

The EC4 compressive resistances of CFHSST stub columns were then calculated and compared against the experimentally and numerically derived load-carrying capacities, with the mean test (or FE) to EC4 predicted resistance ratio $N_u/N_{u,EC4}$ and the corresponding COV reported in Table 6, from which it may be concluded that the European code EN 1994-1-1 [18] generally yields precise and consistent resistance predictions for the new CFHSST stub columns. The test (or FE) to EC4 predicted resistance ratios $N_u/N_{u,EC4}$ are also plotted against the corresponding flat width-to-thickness ratios c/t of the most slender constituent plate elements of the outer high-chromium stainless steel tubes, and shown in Fig. 9. The $N_u/N_{u,EC4}$ ratios are shown to display a 'V-shaped' distribution, revealing that EC4 offers better resistance predictions for CFHSST stub columns with tube dimensions falling within the intermediate range of c/t than those with tube sizes in the high and low ranges of c/t. For CFHSST stub columns with stocky outer high-chromium stainless steel tubes (i.e. in the low range of c/t), the conservatism of the EC4 resistance predictions can be principally attributed to the lack of proper consideration of the material strain hardening of the outer stocky stainless steel tube. With regards to CFHSST stub columns with slender outer tubes falling within the high range of c/t, the conservative EC4 resistance predictions mainly result from the neglect of the favourable effect of the concrete infill on restraining the inward deformation of the outer stainless steel tube and thus delaying its occurrence of local buckling.

4.4 AS 5100 [19]

The Australian standard AS 5100 [19] employs the same formulation for the determination of cross-section compression resistances of square and rectagular CFST stub columns as that given in the European code EN 1994-1-1 [18], but with different flat width-to-thickness limit λ_{AS} between non-slender and slender internal plate elements and effective width expression. In this study, the geometric limit between non-slender and slender internal plate elements was again modified for stainless steel, i.e. with the material 0.2% proof stress replacing the yield

stress, as given in Eq. (11), and the effective width expression for cold-formed stainless steel tubular sections, set out in the Australian/New Zealand standard AS/NZS 4673 [41] for stainless steel structures, was adopted herein, as shown in Eq. (12).

$$\frac{c}{t} \le \lambda_{AS} = 40\left(\frac{250}{\sigma_{0.2}}\right)^{0.5} \tag{11}$$

$$\rho = \frac{1}{\bar{\lambda}_p} - \frac{0.22}{\bar{\lambda}_p^{\,2}} \quad \text{for } \bar{\lambda}_p > 0.673 \tag{12}$$

Quantitative evaluation of the AS cross-section compression capacity predictions was reported in Table 6, with the mean test (or FE) to predicted load-carrying capacity ratio $N_u/N_{u,AS}$ of 1.053 and the corresponding COV equal to 0.046, indicating that the AS 5100 design rules are applicable to the new concrete-filled high-chromium stainless steel tube stub columns, and also shown to result in slightly more precise resistance predictions than the EC4 design provisions. The experimental (or numerical) to AS predicted resistance ratios $N_u/N_{u,AS}$ are also plotted against the corresponding c/t ratios of the most slender plate elements of the outer high-chromium stainless steel tubes in Fig. 10, displaying a similar 'V-shaped' distribution as the test (or FE) to EC4 predicted resistance ratios $N_u/N_{u,EC4}$; the AS capacity predictions were shown to be relatively more conservative for CFHSST stub columns with the outer tube dimensions falling within the high and low flat width-to-thickness ranges than those with the outer tube sizes in the intermediate geometric dimension range.

4.5 Modifications to the codified design provisions

The current design standards were generally found to result in conservative compression resistance predictions for square and rectangular CFHSST stub columns with slender outer tubes, which can be attributed mainly to the neglect of the favourable effect of the concrete infill on delaying the local buckling of the outer stainless steel tube. In comparison with unfilled (bare) steel SHS and RHS stub columns, where the local buckling failure mode is featured by alternating inward and outward deformations of the adjacent plate elements, their concrete-filled counterparts display a higher local buckling failure mode with only outward deformation for all the four constituent plate elements. However, the European code EN 1994-1-1 [18] and Australian standard AS 5100 [19] employ the buckling coefficient k=4, originally derived for plate elements with a two-way elastic critical local buckling mode, in the calculation of the slendernesses and effective widths of plate elements with a higher unidirectional local buckling mode, thus leading to an underestimation of the cross-section effective compression resistances of the outer high-chromium stainless steel tubes of CFHSST stub columns. Bradford et al. [42] derived a new buckling coefficient k=10.67 for the constituent plate elements of concrete-filled steel tubes with outward only buckling mode. Modifications were thus made herein to the current EC4 and AS 5100 design provisions through the use of the buckling coefficient k=10.67 in calculating the effective cross-section areas of the outer high-chromium stainless steel tubes of CFHSST stub columns. Moreover, the EC4 and AS 5100 limits between non-slender and slender internal plate elements were also revised accordingly, through (i) setting Eq. (10) for plate element slenderness equal to the respective limiting slendernesses of 0.65 and 0.673, and

(ii) solving for the c/t ratios. The revised EC4 and AS 5100 limits between non-slender and slender internal plate elements, respectively denoted as $\lambda_{EC4,r}$ and $\lambda_{AS,r}$, are given by Eqs (13) and (14).

$$\frac{c}{t} \le \lambda_{EC4,r} = 60\left(\frac{235}{\sigma_{0.2}}\frac{E}{210000}\right)^{0.5} \tag{13}$$

$$\frac{c}{t} \le \lambda_{AS,r} = 63\left(\frac{235}{\sigma_{0.2}}\frac{E}{210000}\right)^{0.5} \tag{14}$$

The accuracy the of the revised EC4 and AS 5100 design rules, together with the corresponding original design provisions, was evaluated herein for CFHSST stub columns with slender outer high-chromium stainless steel tubes. As shown in Table 7, the mean ratios of the experimental (or FE) load-carrying capacities to the predicted resistances from the revised EC4 and AS 5100 design provisions ($N_u/N_{EC4,r}$ and $N_u/N_{AS,r}$) are equal to 1.037 and 1.006, respectively, with the COVs of 0.013 and 0.015, in comparison with the mean ratios of N_u/N_{EC4} and N_u/N_{AS} equal to 1.111 and 1.048 with COVs of 0.024 and 0.032 derived from the original EC4 and AS 5100 design rules. The results of the evaluation indicate that the revised EC4 and AS 5100 design provisions, incorporating a more proper buckling coefficient k=10.67 and revised c/t limits between non-slender and slender internal plate elements, offer a notable improvement over the original codified design rules in the resistance predictions of CFHSST stub columns with slender outer high-chromium stainless steel tubes; this is also evident in Figs 9 and 10, where the test (and FE) to predicted resistance ratios determined from both the revised and original codified design provisions are plotted against the cross-section c/t ratios.

5. Conclusion

The compressive behaviour and load-carrying capacities of the new concrete-filled high-chromium stainless steel tube (CFHSST) stub columns was studied in this paper through a thorough experimental and finite element modelling programme. The testing programme was carried out on 15 CFHSST stub columns with high-chromium stainless steel tubes of five different cross-section sizes and concrete infill of three grades as well as 5 (reference) bare high-chromium stainless steel tube stub columns. The test setup and procedure were described in detail, and the experimental observations, including the ultimate loads, load–end shortening curves and failure modes, were fully reported. This was followed by a numerical modelling programme, where finite element models were firstly developed and validated against the CFHSST stub column test results, and then utilised to perform numerical parametric studies to expand the experimental data pool on CFHSST stub columns over a wider range of cross-section sizes. Both of the derived test data and generated numerical parametric study results were adopted to evaluate the applicability of the established design provisions for concrete-filled carbon steel tube stub columns, as set out in the American specification AISC 360-16 [17], European code EN 1994-1-1 [18] and Australian standard AS 5100 [19], to the design of the new concrete-filled high-chromium stainless steel tube stub columns. It was generally found that all the examined codified design rules can be safely applied to the new high-

chromium stainless steel composite stub columns, though with slightly conservative resistance predictions for those with stocky and slender outer tubes. Modifications to the EC4 and AS 5100 design rules were then made, and shown to yield an improved level of resistance predictions for CFHSST stub columns with slender outer tubes.

Acknowledgements

The authors would like to thank Outokumpu Oyj for providing high-chromium grade EN 1.4420 stainless steel plates and Stalatube Oy for fabricating SHS and RHS from the plates, and are also grateful to Mr. Subasanran Chelladurai and Mr. Cheng Hoon Tui for their assistances during testing. The research work described in this paper is financially support by the Academic Research Fund (AcRF) Tier 1 Grant (Project ID: 2018-T1-001-243) from the Ministry of Education, Singapore.

References

[1] Uy B, Tao Z, Han LH. Behaviour of short and slender concrete-filled stainless steel tubular columns. Journal of Constructional Steel Research. 2011;67:360-78.

[2] Young B, Ellobody E. Experimental investigation of concrete-filled cold-formed high strength stainless steel tube columns. Journal of Constructional Steel Research. 2006;62:484-92.

[3] Lam D, Gardner L. Structural design of stainless steel concrete filled columns. Journal of Constructional Steel Research. 2008;64:1275-82.

[4] Dabaon MA, El-Boghdadi MH, Hassanein MF. Experimental investigation on concrete-filled stainless steel stiffened tubular stub columns. Engineering Structures. 2009;31:300-7.

[5] Yang Y-F, Ma G-L. Experimental behaviour of recycled aggregate concrete filled stainless steel tube stub columns and beams. Thin-Walled Structures. 2013;66:62-75.

[6] Li YL, Zhao XL, Singh RKR, Al-Saadi S. Experimental study on seawater and sea sand concrete filled GFRP and stainless steel tubular stub columns. Thin-Walled Structures. 2016;106:390-406.

[7] Li YL, Zhao XL, Raman Singh RK, Al-Saadi S. Tests on seawater and sea sand concrete-filled CFRP, BFRP and stainless steel tubular stub columns. Thin-Walled Structures. 2016;108:163-84.

[8] Ellobody E, Ghazy MF. Experimental investigation of eccentrically loaded fibre reinforced concrete-filled stainless steel tubular columns. Journal of Constructional Steel Research. 2012;76:167-76.

[9] Tokgoz S. Tests on plain and steel fiber concrete-filled stainless steel tubular columns. Journal of Constructional Steel Research. 2015;114:129-35.

[10] Han L-H, Chen F, Liao F-Y, Tao Z, Uy B. Fire performance of concrete filled stainless steel tubular columns. Engineering Structures. 2013;56:165-81.

[11] Tao Z, Ghannam M, Song T-Y, Han L-H. Experimental and numerical investigation of concrete-filled stainless steel columns exposed to fire. Journal of Constructional Steel Research. 2016;118:120-34.

[12] Chen Y, He K, Han S, Wei J. Experimental investigation of square concrete filled stainless steel tubular stub columns after exposure to elevated temperatures. Thin-Walled Structures. 2018;130:12-31.

[13] Signorelli R, Wegrelius L, Ohligschläger T. Corrosion resistance of Supra 316plus – a comparison with 1.4404 and 1.4432. In: Proceeding of 9th European Stainless Steel Conference & 5th European Duplex Stainless Steel Conference: 2017 May 25-27; Bergamo (Italy). Milano: Associazione Italiana di Metallurgia; 2017.

[14] Liang Y, Manninen T, Zhao O, Walport F, Gardner L. Elevated temperature material properties of a new high-chromium austenitic stainless steel. Journal of Constructional Steel Research. 2019;152:261-73.

[15] Sun Y, Zhao O. Material response and local stability of high-chromium stainless steel welded I-sections. Engineering Structures. 2019;178:212-26.

[16] EN 10028-7: 2016. Flat products made of steels for pressure purposes – part 7: stainless steels. Brussels: European Committee for Standardization (CEN); 2014.

[17] American Institute of Steel Construction (AISC). Specification for structural steel buildings. AISC 360-16, Chicago (IL); 2016.

[18] EN 1994-1-1:2004. Eurocode 4: design of composite steel and concrete structures – Part 1-1: General rules and rules for buildings. Brussels: European Committee for Standardization (CEN); 2004.

[19] Standards Australia. Bridge design, Part 6: steel and composite construction. AS5100.6-2004, Sydney, Australia; 2004.

[20] Han L-H. Tests on stub columns of concrete-filled RHS sections. Journal of Constructional Steel Research. 2002;58:353-72.

[21] EN ISO 6892-1. Metallic materials – tensile testing – Part 1: Method of test at room temperature. Brussels: European Committee for Standardization (CEN); 2009.

[22] Ramberg W, Osgood WR. Description of stress–strain curves by three parameters. Technical note no. 902. Washington DC: National Advisory Committee for Aeronautics; 1943.

[23] Hill HN. Determination of stress–strain relations from offset yield strength values. Technical note no. 927. Washington DC: National Advisory Committee for Aeronautics; 1944.

[24] Mirambell E, Real E. On the calculation of deflections in structural stainless steel beams: an experimental and numerical investigation. Journal of Constructional Steel Research. 2000;54:109-33.

[25] Rasmussen KJR. Full-range stress–strain curves for stainless steel alloys. Journal of Constructional Steel Research. 2003;59:47-61.

[26] Gardner L, Ashraf M. Structural design for non-linear metallic materials. Engineering Structures. 2006;28:926-34.

[27] EN 12390-3:2009. Testing hardened concrete – Part 3: Compressive strength of test specimens. Brussels: European Committee for Standardization (CEN); 2009.

[28] Han L-H, Yao G-H, Zhao X-L. Tests and calculations for hollow structural steel (HSS) stub columns filled with self-consolidating concrete (SCC). Journal of Constructional Steel Research. 2005;61:1241-69.

[29] dos Santos GB, Gardner L, Kucukler M. A method for the numerical derivation of plastic collapse loads. Thin-Walled Structures. 2018;124:258-77.

[30] Wang F, Young B, Gardner L. Compressive testing and numerical modelling of concrete-filled double skin CHS with austenitic stainless steel outer tubes. Thin-Walled Structures: in press.

[31] Tao, Z., Han, L. H., Zhao, X. L. Tests on stub columns of concrete filled double skin rectangular hollow sections. Proc.,4th Int. conf. on Thin-Walled Struct. 2004; 885-92.

[32] ABAQUS. ABAQUS/standard user's manual volumes I–III and ABAQUS CAE manual. Version 6.12. Pawtucket (USA): Hibbitt, Karlsson & Sorensen, Inc; 2012.

[33] Tao Z, Uy B, Liao F-Y, Han L-H. Nonlinear analysis of concrete-filled square stainless steel stub columns under axial compression. Journal of Constructional Steel Research. 2011;67:1719-32.

[34] Tao Z, Wang Z-B, Yu Q. Finite element modelling of concrete-filled steel stub columns under axial compression. Journal of Constructional Steel Research. 2013;89:121-31.

[35] Ye Y, Zhang S-J, Han L-H, Liu Y. Square concrete-filled stainless steel/carbon steel bimetallic tubular stub columns under axial compression. Journal of Constructional Steel Research. 2018;146:49-62.

[36] American Concrete Institute. Building code requirements for structural concrete. ACI 318-14, Farmington Hills, MI; 2014.

[37] CEB-FIP (Euro-International Committee for Concrete (CEB)-International Federation for Prestressing (FIP).). Model Code for concrete structures. (CEB-FIP MC 2010). London, U.K.: Thomas Telford; 2010.

[38] Gardner L, Nethercot DA. Numerical Modeling of Stainless Steel Structural Components—A Consistent Approach. Journal of Structural Engineering. 2004;130:1586-601.

[39] Dawson RG, Walker AC. Post-buckling of geometrically imperfect plates. Journal of the Structural Division. 1972;98:75-94.

[40] EN 1993-1-4:2006+A1:2015. Eurocode 3: design of steel structures – part 1. 4: general rules – supplementary rules for stainless steels, including amendment A1 (2015). Brussels: European Committee for Standardization (CEN); 2015.

[41] AS/NZS 4673. Cold-formed stainless steel structures. Sydney: AS/NZS 4673:2001; 2001.

[42] Bradford MA, Wright HD, Uy B. Local Buckling of the Steel Skin in Lightweight Composites Induced by Creep and Shrinkage. Advances in Structural Engineering. 1998;2:25-34.

Table 1 Chemical compositions of stainless steel grades 1.4301, 1.4404 and 1.4420.

Grade	C (%)	Si (%)	Mn (%)	P (%)	S (%)	N (%)	Cr (%)	Mo (%)	Ni (%)
1.4301	≤0.07	≤1.00	≤2.00	0.045	0.015	≤0.10	17.5 – 19.5	–	8.0 – 10.5
1.4404	≤0.03	≤1.00	≤2.00	0.045	0.015	≤0.10	16.5 – 18.5	2.0 – 2.5	10.0 – 13.0
1.4420	≤0.07	≤1.00	≤2.00	0.045	0.015	0.14 – 0.25	19.5 – 21.5	0.5 – 1.5	8.0 – 9.5

Table 2 Measured geometric dimensions of specimens.

Specimen	h (mm)	b (mm)	t (mm)	r_i (mm)	L (mm)	A_s (mm^2)	A_c (mm^2)	ξ
SHS 100×100×3-C0	100.5	99.9	3.00	4.5	299	1135	–	–
SHS 100×100×3-C40	99.8	99.3	3.00	4.5	299	1128	8734	0.96
SHS 100×100×3-C60	101.0	100.5	3.00	4.5	299	1142	8960	0.68
SHS 100×100×3-C80	101.0	100.5	3.00	4.5	299	1142	8960	0.54
SHS 120×120×5-C0	120.6	119.4	4.96	6.5	358	2206	–	–
SHS 120×120×5-C40	121.0	120.5	4.98	6.5	358	2229	12238	1.18
SHS 120×120×5-C60	120.0	120.0	4.98	6.5	359	2214	12073	0.85
SHS 120×120×5-C80	120.5	119.5	4.96	6.5	357	2206	12081	0.67
SHS 150×150×5-C0	150.2	149.6	4.96	6.5	449	2799	–	–
SHS 150×150×5-C40	150.0	149.5	4.97	6.5	447	2802	19511	0.95
SHS 150×150×5-C60	150.0	149.5	4.96	6.5	449	2796	19516	0.68
SHS 150×150×5-C80	150.0	149.5	4.98	6.5	449	2807	19505	0.54
RHS 100×50×5-C0	100.1	49.7	5.01	6.0	298	1327	–	–
RHS 100×50×5-C40	100.1	49.7	4.99	6.0	299	1323	3549	2.42
RHS 100×50×5-C60	100.2	49.7	4.98	6.0	299	1321	3555	1.74
RHS 100×50×5-C80	100.1	49.7	5.02	6.0	299	1330	3541	1.39
RHS 150×100×5-C0	149.2	101.0	4.97	6.5	449	2312	–	–
RHS 150×100×5-C40	149.5	100.3	4.99	6.5	448	2316	12565	1.17
RHS 150×100×5-C60	149.8	100.4	4.98	6.5	447	2316	12611	0.84
RHS 150×100×5-C80	149.7	100.3	4.95	6.5	445	2301	12602	0.66

Table 3 Measured key material properties from tensile coupon tests.
(a) Flat coupons

Cross section	E (GPa)	$\sigma_{0.2}$ (MPa)	σ_u (MPa)	ε_u (%)	n	m
SHS 100×100×3	217	365	707	39	6.0	2.8
SHS 120×120×5	201	317	665	44	6.3	2.7
SHS 150×150×5	210	324	673	44	7.8	2.7
RHS 100×50×5	199	322	671	44	3.4	2.7
RHS 150×100×5	201	321	669	42	6.0	2.7

(b) Corner coupons

Cross section	E (GPa)	$\sigma_{0.2}$ (MPa)	σ_u (MPa)	ε_u (%)	n	m
SHS 100×100×3	208	503	781	27	1.7	3.3
SHS 120×120×5	195	560	795	26	2.3	3.5
SHS 150×150×5	203	548	805	25	1.6	3.4
RHS 100×50×5	197	525	759	26	2.6	3.4
RHS 150×100×5	195	554	759	24	1.9	3.6

Table 4 Mixture proportion of concretes.

Grade	Gravel (kg)	Sand (kg)	Cement (kg)	Water (kg)	Silica fume (kg)	Superplasticizer (kg)
C40	795	789	462	240	–	–
C60	795	789	570	205	–	–
C80	736	746	457	189	67	5

Table 5 Summary of experimental and numerical results.

Specimen	$N_{u,test}$ (kN)	δ_u (mm)	DI	$N_{u,FE}$ (kN)	$N_{u,FE}/N_{u,test}$
SHS 100×100×3-C0	433	1.31	1.44	395	0.913
SHS 100×100×3-C40	830	1.40	3.49	881	1.061
SHS 100×100×3-C60	1004	1.49	1.57	1042	1.038
SHS 100×100×3-C80	1162	1.25	1.55	1182	1.017
SHS 120×120×5-C0	898	3.31	1.65	918	1.022
SHS 120×120×5-C40	1373	2.79	>4.58	1403	1.022
SHS 120×120×5-C60	1566	2.10	5.08	1605	1.025
SHS 120×120×5-C80	1840	1.58	1.71	1808	0.983
SHS 150×150×5-C0	1031	3.04	1.56	1051	1.019
SHS 150×150×5-C40	1860	2.07	>4.41	1968	1.058
SHS 150×150×5-C60	2218	1.51	2.13	2320	1.046
SHS 150×150×5-C80	2612	1.31	1.39	2640	1.011
RHS 100×50×5-C0	617	6.40	2.10	607	0.984
RHS 100×50×5-C40	720	3.17	>3.20	710	0.986
RHS 100×50×5-C60	768	2.25	>4.10	755	0.983
RHS 100×50×5-C80	837	1.71	>4.94	799	0.955
RHS 150×100×5-C0	879	3.76	2.04	890	1.012
RHS 150×100×5-C40	1419	2.42	>4.59	1459	1.028
RHS 150×100×5-C60	1643	1.80	1.78	1675	1.019
RHS 150×100×5-C80	1920	1.38	1.54	1891	0.985
				Mean	1.008
				COV	0.035

Table 6 Comparison of test and FE results with predicted resistances for CFHSST stub columns.

No. of tests:15	AISC 360-16	EC4	AS 5100
No. of FE simulations: 210	$N_u/N_{u,AISC}$	$N_u/N_{u,EC4}$	$N_u/N_{u,AS}$
Mean value	1.155	1.087	1.053
COV	0.043	0.044	0.046

Table 7 Comparison of test and FE results with predicted resistance for CFHSST stub columns with slender outer tubes.

No. of data: 60	EC4	AS 5100	Revised EC4	Revised AS 5100
	$N_u/N_{u,EC4}$	$N_u/N_{u,AS}$	$N_u/N_{u,EC4,r}$	$N_u/N_{u,AS,r}$
Mean value	1.111	1.048	1.037	1.006
COV	0.024	0.032	0.013	0.015

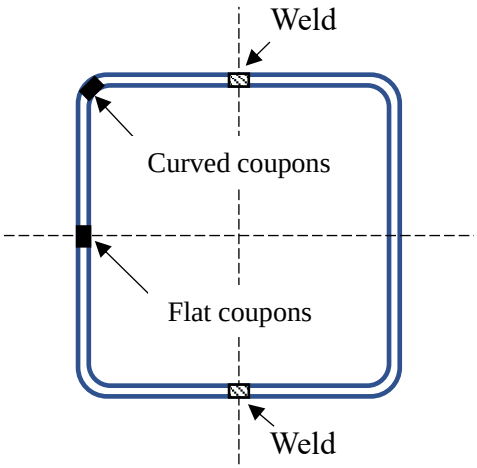

Fig. 1. Locations of tensile coupons.

Fig. 2. Tensile coupon test rig.

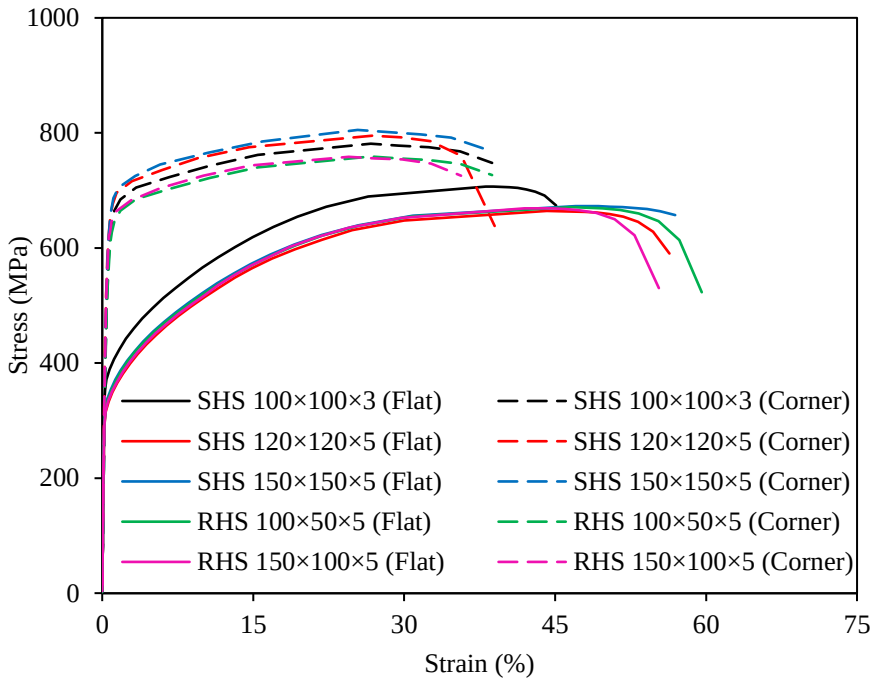

Fig. 3. Measured stress–strain curves of high-chromium grade EN 1.4420 stainless steel tubes.

Fig. 4. Stub column test setup.

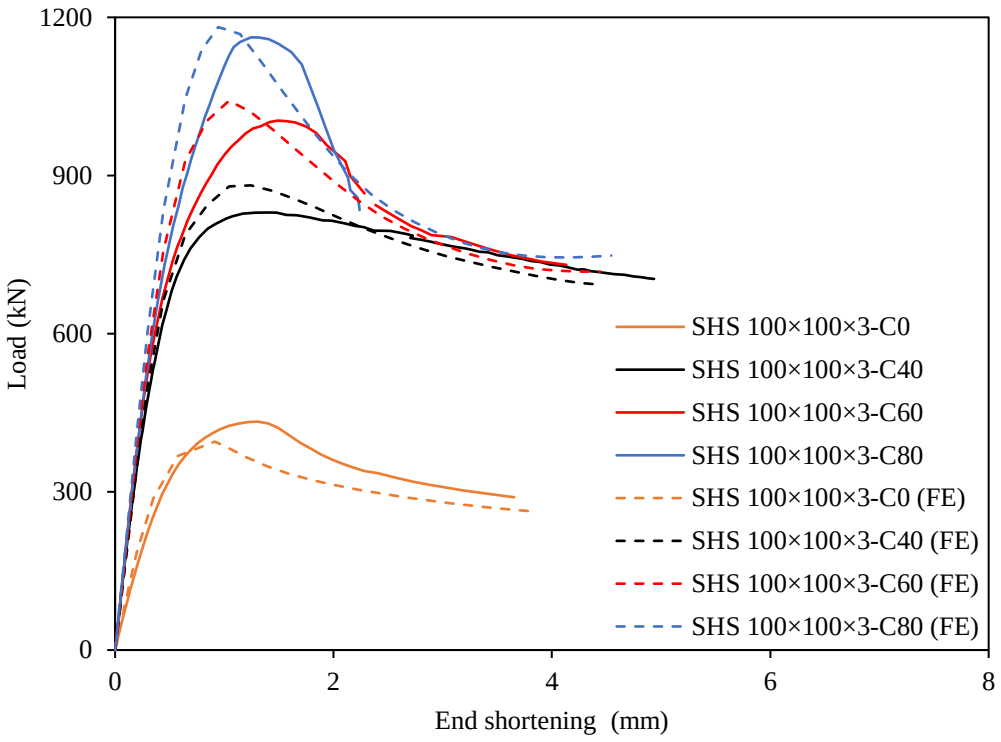

(a) Specimen series with outer tubes of SHS 100×100×3.

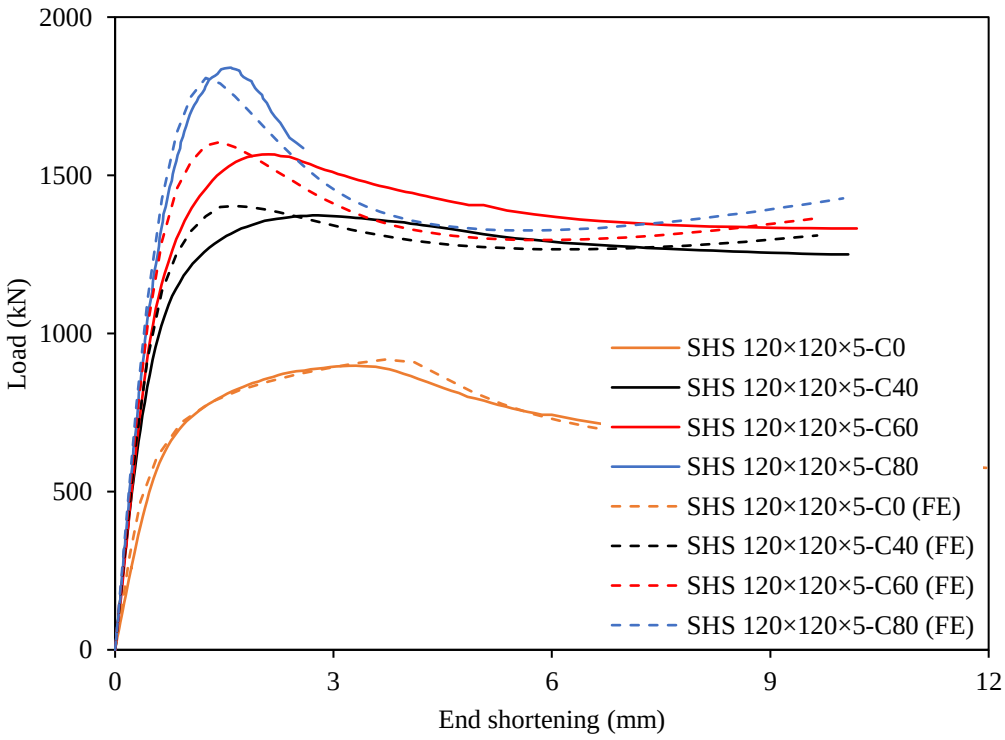

(b) Specimen series with outer tubes of SHS 120×120×5.

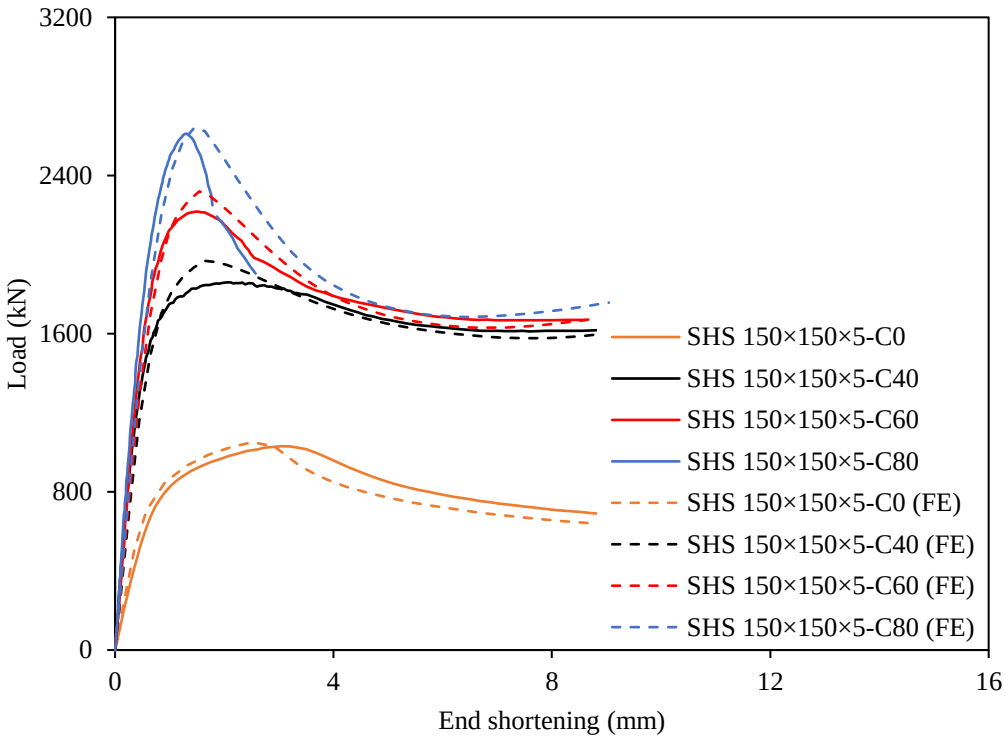

(c) Specimen series with outer tubes of SHS 150×150×5.

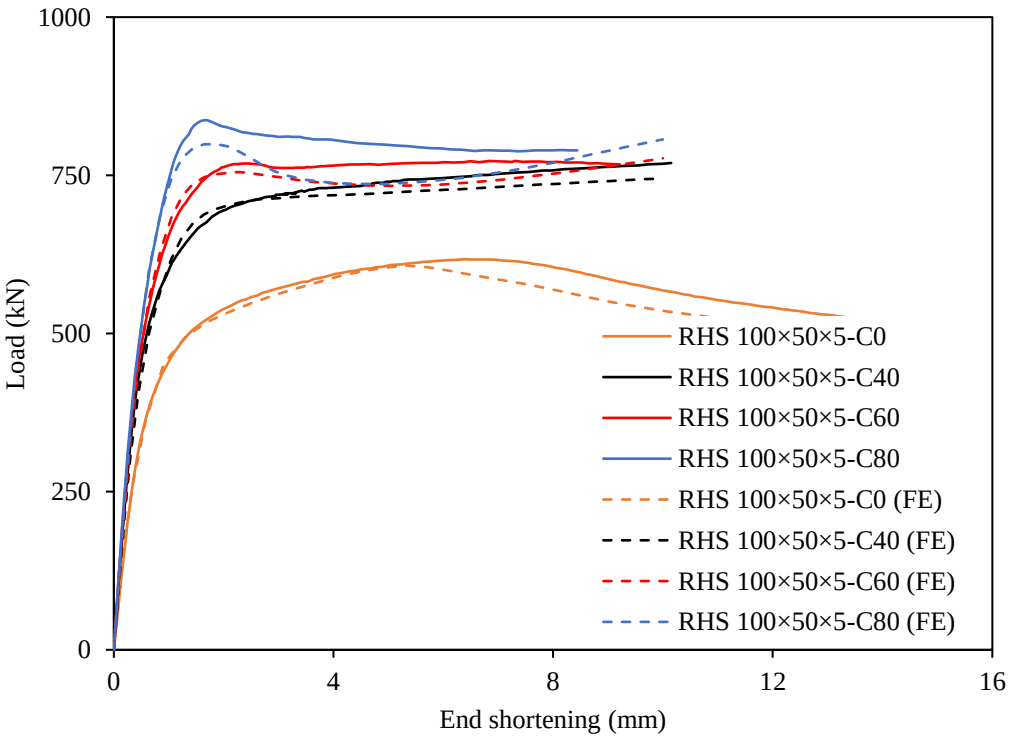

(d) Specimen series with outer tubes of RHS 100×50×5.

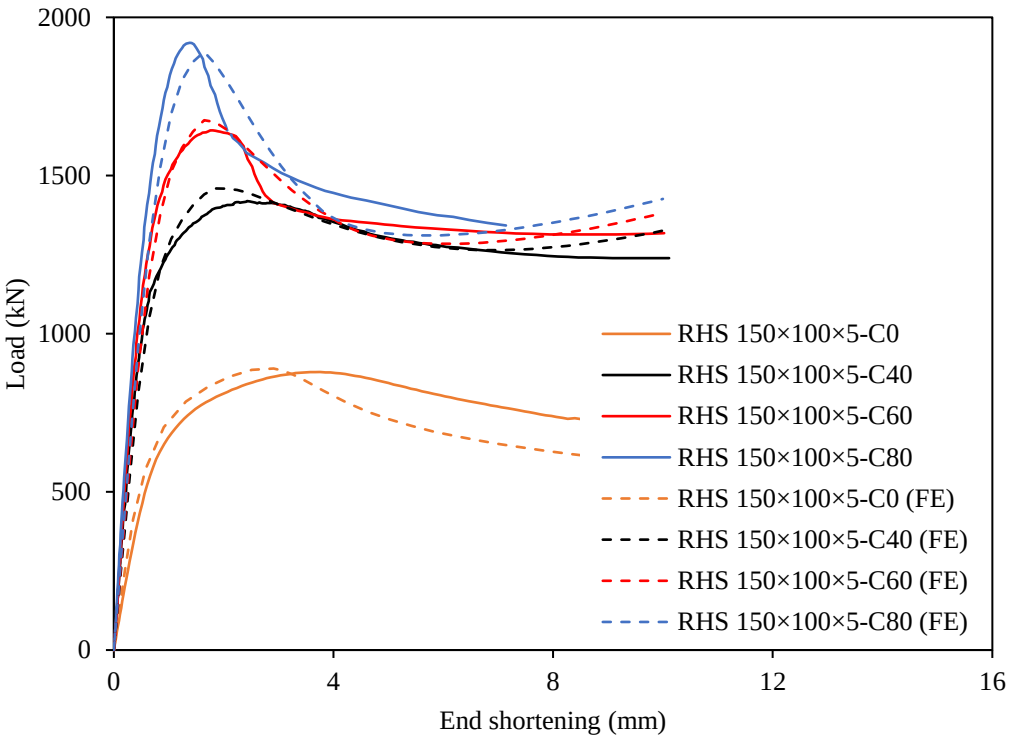

(e) Specimen series RHS 150×100×5.

Fig. 5. Load–end shortening curves for CFHSST stub column specimens.

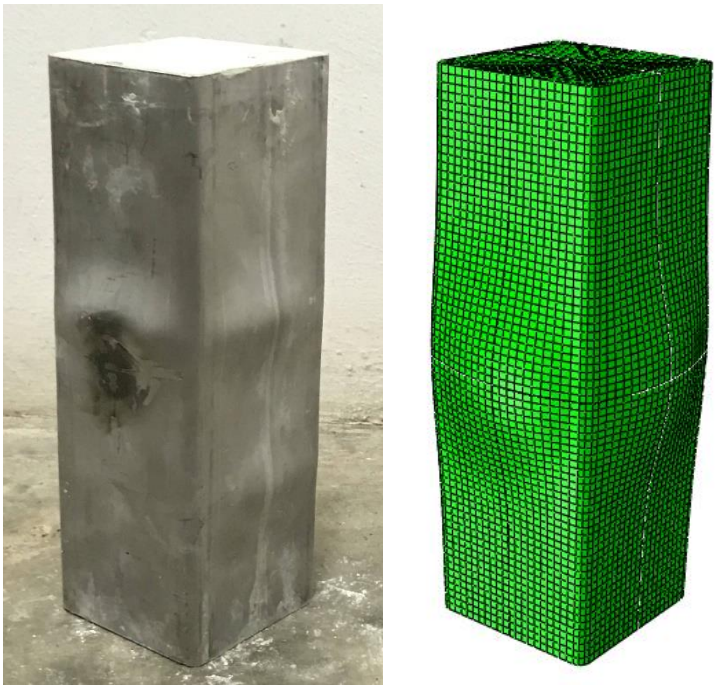

Fig. 6. Experimental and numerical failure modes for CFHSST stub specimen SHS 100×100×3-C40.

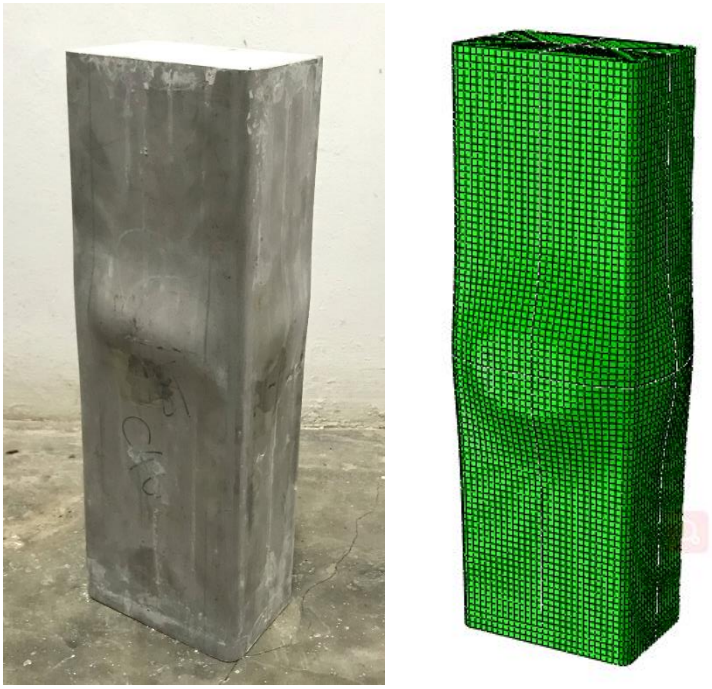

Fig. 7. Experimental and numerical failure modes for CFHSST stub specimen RHS 150×100×5-C40.

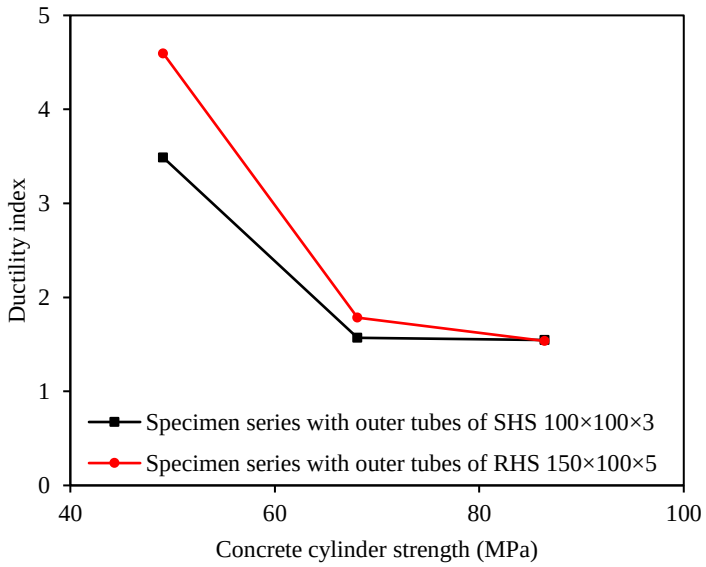

Fig. 8. Ductility indices of CFHSST stub columns series with outer tubes of SHS 100×100×3 and RHS 150×100×5.

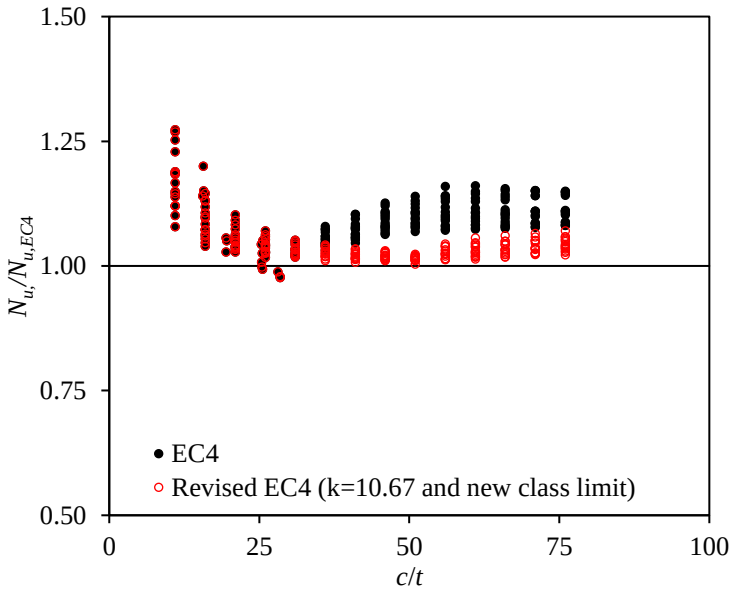

Fig. 9. Comparison of test and FE results with resistance predictions from original and revised EN 1994-1-1.

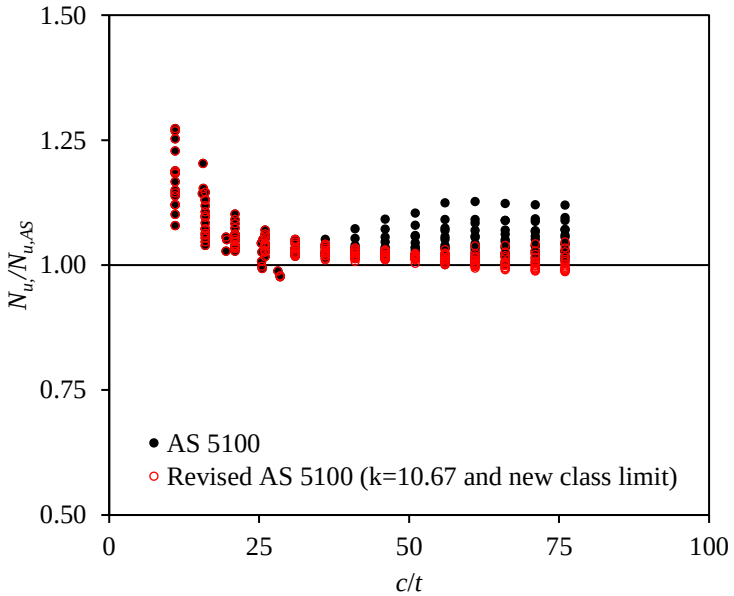

Fig. 10. Comparison of test and FE results with resistance predictions from original and revised AS 5100.